# Phosphine Oxide-Functionalized Terthiophene Redox Systems

How to cite: *Angew. Chem. Int. Ed.* **2023**, *62*, e202304600
doi.org/10.1002/anie.202304600

Redox Chemistry | Hot Paper

# Phosphine Oxide-Functionalized Terthiophene Redox Systems

*Daniel Käch, Aurelio C. Gasser, Lionel Wettstein, Clara Schweinzer, and Máté J. Bezdek**

**Abstract:** Main group systems capable of undergoing controlled redox events at extreme potentials are elusive yet highly desirable for a range of organic electronics applications including use as energy storage media. Herein we describe phosphine oxide-functionalized terthiophenes that exhibit two reversible $1e^-$ reductions at potentials below −2 V vs $Fc/Fc^+$ (Fc = ferrocene) while retaining high degrees of stability. A phosphine oxide-functionalized terthiophene radical anion was synthesized in which the redox-responsive nature of the platform was established using combined structural, spectroscopic, and computational characterization. Straightforward structural modification led to the identification of a derivative that exhibits exceptional stability during bulk $2e^-$ galvanostatic charge–discharge cycling and enabled characterization of a $2e^-$ redox series. A new multi-electron redox system class is hence disclosed that expands the electrochemical cell potential range achievable with main group electrolytes without compromising stability.

Redox systems based on main group elements are emerging as next-generation building blocks for organic batteries, electrochromic materials, magnets, photovoltaics, and sensors.[1,2] Although they are attractive from economic and sustainability perspectives,[3] main group elements typically feature a lower density of redox states compared to transition metals and consequently yield difficult-to-control, highly reactive radical species upon electron transfer.[4] The discovery of new main group systems capable of undergoing controlled redox processes therefore continues to be of both fundamental and applied interest, and research on persistent main group radicals continues apace.[5]

Main group redox systems could prove especially valuable in energy storage devices, particularly as chargeable electrolytes for redox flow batteries (RFBs).[6,7] Owing to their relatively high-lying unoccupied molecular orbitals, main group electrolytes could maximize theoretical cell voltages by virtue of charge/discharge processes that take place at extreme potentials near the edge of organic solvents' electrochemical windows (e.g. 6.1 V in MeCN vs 1.2 V in water).[8] For instance, organic redox systems such as viologens (**I**$^{2+}$),[9] quinones (**II**),[10] 2,2′-bipyrimidines (**III**)[11] and their functionalized variants[12–16] can undergo multi-electron, reversible reduction at low potentials of −1 to −2 V in MeCN and could unlock cell voltages that are inaccessible under aqueous conditions (Scheme 1A). However, the intrinsically high reactivity of organic radicals means that there exists a tradeoff in such systems between stored electrochemical energy and stability, wherein redox processes at more negative potentials are typically achieved at the expense of electrolyte lifetime. While systematic studies are emerging that aim to identify and rationally mitigate organic electrolyte decomposition,[11] it remains challenging to design new structural motifs that are capable of multi-electron storage at extreme electrochemical potentials (< −2 V) yet are sufficiently stable to withstand continuous redox cycling.

Oligothiophenes such as terthiophene (TTH) are among the most well-studied structural motifs in organic electronics[17] yet are surprisingly underexplored as molecular redox systems.[18,19] Although they offer the possibility

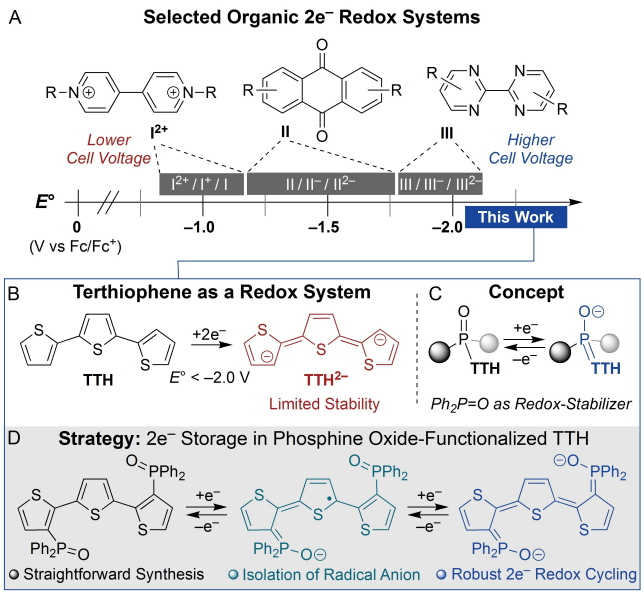


***Scheme 1.*** A) Selected examples of organic redox systems capable of $2e^-$ storage together with corresponding redox couple ranges. B) The opportunity and challenge of $2e^-$ storage in terthiophene (TTH). C) Phosphine oxides as redox stabilizers. D) The strategy reported in this work.

[*] D. Käch, A. C. Gasser, L. Wettstein, C. Schweinzer, Prof. Dr. M. J. Bezdek
Department of Chemistry and Applied Biosciences, ETH Zürich
Vladimir-Prelog-Weg 1, 8093 Zürich (Switzerland)
E-mail: mbezdek@ethz.ch

of multi-electron storage at extreme negative potentials and could therefore exhibit very high theoretical cell voltages in the context of RFB applications,[20] studies on the electrochemical reduction of oligothiophenes have established the instability of formed anions.[21] To enable redox cycling over extended time periods and hence application in device settings, introduction of functionalities would be necessary that can stabilize the quinoidal anionic form of oligothiophenes (Scheme 1B). In contrast to conventional electron withdrawing groups such as nitro and cyano substituents that tend to compromise the negative redox potentials of oligothiophenes,[22–24] we hypothesized that diaryl phosphine oxides should be well-suited for this purpose. Widely studied electron acceptors in the field of organic electronics,[25] phosphine oxides feature a unique P–O bonding scenario wherein negative hyperconjugation gives rise to an increased relative electronegativity at P and hence the overall electron-accepting character of the phosphine oxide moiety (Scheme 1C).[26,27] Herein we leverage this attribute and demonstrate that phosphine oxide-functionalized terthiophenes undergo fully reversible net $2e^-$ reduction at extreme negative potentials (Scheme 1D). We detail the solid-state and electronic structure of a crystalline phosphine oxide-functionalized terthiophene radical anion and present the tuning of its redox properties via structural variation at the terthiophene backbone. Finally, we show that this fundamentally new class of electrolytes can undergo remarkably robust $2e^-$ charge–discharge cycling for extended periods at low potentials.

Straightforward oxidation of 3,3″-$(PPh_2)_2$-TTH (**1**)[28,29] with excess $H_2O_2$ afforded the corresponding phosphine oxide-functionalized terthiophene 3,3″-$(P(O)Ph_2)_2$-TTH (**2**) as a crystalline yellow solid in 90 % yield (Scheme 2A). The $^1H$ and $^{31}P\{^1H\}$ NMR spectra of **2** in $CDCl_3$ exhibit the number of resonances consistent with an overall $C_{2v}$ molecular symmetry in solution, establishing free rotation about the inter-thiophene C–C bonds. The electrochemical properties of **2** were probed by cyclic voltammetry (CV) to experimentally assess its suitability for electron storage. The cyclic voltammogram of **2** was recorded in DME solution at room temperature and exhibits an irreversible anodic wave at +0.93 V vs $Fc/Fc^+$ (Fc = ferrocene) as well as two reversible cathodic waves with half-wave potentials ($E_{1/2}$) of −2.14 and −2.40 V vs $Fc/Fc^+$ (Scheme 2B). While the wave at +0.93 V is assigned to a one-electron oxidation, the waves at −2.14 and −2.40 V are relevant to the ability of **2** to store electrons and correspond to reduction events. The fully reversible nature of these cathodic features is retained even after extended cycling as shown in Scheme 2C and is a notable attribute of **2**. By contrast, compound **1**, unfunctionalized TTH and 3,3″-$Br_2$-TTH all exhibit either irreversible or quasi-reversible cathodic features while the cyano analog 3,3″-$CN_2$-TTH degrades upon repeated cycling despite showing reversible waves at −1.94 and −2.25 V (Figures S34–S37). Changing the supporting electrolyte from [(*n*-Bu)$_4$N][$PF_6$] to [Li][$PF_6$] or [K][$PF_6$] resulted in a small anodic $E_{1/2}$ shift for **2**, implying that Lewis acidic ions reversibly interact with its reduced states (Figure S28). Taken together, these observations establish the importance

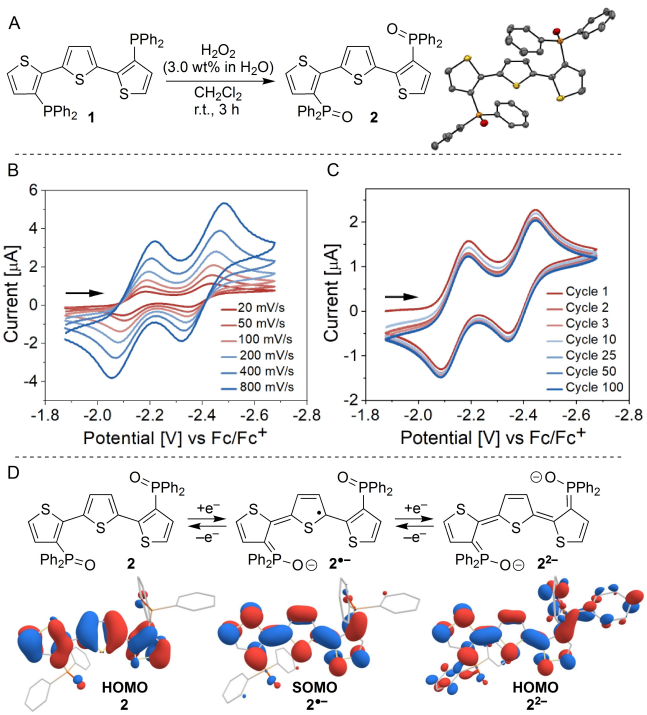


***Scheme 2.*** A) Synthesis of **2** and its solid-state structure with 50 % probability ellipsoids (hydrogen atoms omitted for clarity). B) CV of **2** at various scan rates and C) after extended cycling at 100 $mV\,s^{-1}$ (r.t., 1.0 mM **2**, 0.10 M [(*n*-Bu)$_4$N][$PF_6$] in DME, glassy carbon working electrode). D) DFT-computed sequential one-electron reduction of **2** to generate $\mathbf{2}^{\bullet-}$ and $\mathbf{2}^{2-}$ together with frontier orbital illustrations for each redox state. For $\mathbf{2}^{\bullet-}$, one of several possible radical resonance forms was drawn. Analogous frontier orbitals were computed for possible conformers of **2**, $\mathbf{2}^{\bullet-}$ and $\mathbf{2}^{2-}$ (see Supporting Information for details).

of phosphine oxide functionalization for the well-defined redox chemistry in **2**.

The electronic structure of **2** as well as its one- and two electron reduced analogs ($\mathbf{2}^{\bullet-}$ and $\mathbf{2}^{2-}$) were examined by density functional theory (DFT) calculations at the BP86 level of theory to gain insight into the nature of the $2e^-$ reduction. Consistent with the established influence of reductive (n-type) doping on the electronic structure of oligothiophenes,[30] the highest occupied molecular orbital (HOMO) of **2** suggests aromatic "benzenoidal" character. By contrast, the singly occupied molecular orbital (SOMO) of $\mathbf{2}^{\bullet-}$ and the HOMO of $\mathbf{2}^{2-}$ show a shift towards a "quinoidal" form (Scheme 2D).[31] Unlike **2**, reduced products $\mathbf{2}^{\bullet-}$ and $\mathbf{2}^{2-}$ adopt a planar terthiophene configuration with an increased bond order between thiophene subunits, in line with their quinoidal character. Additionally, an increased P–C bond order was observed between the terthiophene and the diphenylphosphine oxide substituents, supporting their role in the stabilization of reduced terthiophene.

The reversible cathodic electrochemical features observed for **2** also prompted investigation of its chemical reduction. Treatment of **2** with one equivalent of sodium naphthalenide in THF solution at −34 °C resulted in a color change from light yellow to dark blue. The product of the

reaction was identified as the sodium complex [Na(**2**)-(THF)]$_2$ isolated in 57 % yield after recrystallization (Scheme 3A). The structure of [Na(**2**)(THF)]$_2$ was determined by single crystal X-ray diffraction which established a dimeric arrangement in the solid-state. Shown in Scheme 3B, each sodium atom in [Na(**2**)(THF)]$_2$ is coordinated by one terminal and one bridging phosphine oxide moiety as well as a molecule of THF. As indicated by the DFT-computed structure of **2**$^{\bullet-}$, planarization of the terthiophene backbone was observed for [Na(**2**)(THF)]$_2$ alongside several key bond length changes that accompany the reduction. Summarized in Scheme 3B, the observed structural changes include shortening of the $C_{TTH}$–P bonds in [Na(**2**)(THF)]$_2$ (C3–P1, C10–P2) as well as shortening of *inter*-thiophene C–C bonds (C4–C5, C8–C9).[32] Concomitantly, an alternating elongation/contraction pattern is observed for *intra*-thiophene C–C bonds in [Na(**2**)(THF)]$_2$ compared to **2**. These observations

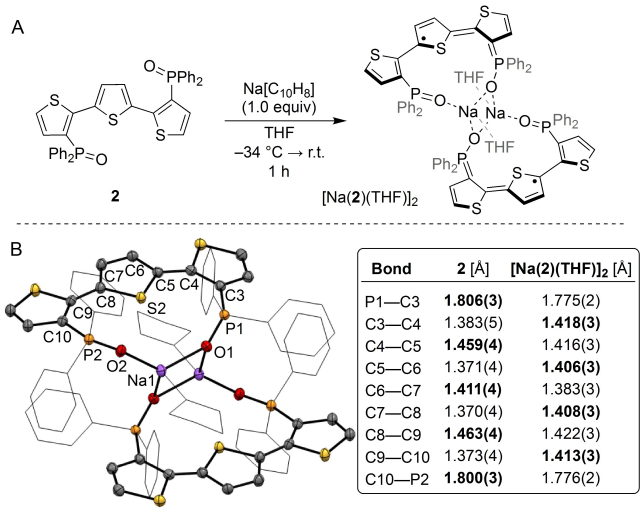


| Bond | 2 [Å] | [Na(2)(THF)]$_2$ [Å] |
|---|---|---|
| P1—C3 | **1.806(3)** | 1.775(2) |
| C3—C4 | 1.383(5) | **1.418(3)** |
| C4—C5 | **1.459(4)** | 1.416(3) |
| C5—C6 | 1.371(4) | **1.406(3)** |
| C6—C7 | **1.411(4)** | 1.383(3) |
| C7—C8 | 1.370(4) | **1.408(3)** |
| C8—C9 | **1.463(4)** | 1.422(3) |
| C9—C10 | 1.373(4) | **1.413(3)** |
| C10—P2 | **1.800(3)** | 1.776(2) |

***Scheme 3.*** A) Synthesis of [Na(**2**)(THF)]$_2$. B) Solid-state structure of [Na(**2**)(THF)]$_2$ with 50 % probability ellipsoids (hydrogen atoms omitted, phenyl substituents and THF solvent molecules represented without probability ellipsoids for clarity). Key bond length changes in comparison to **2** are shown, wherein bond elongation is highlighted in bold.

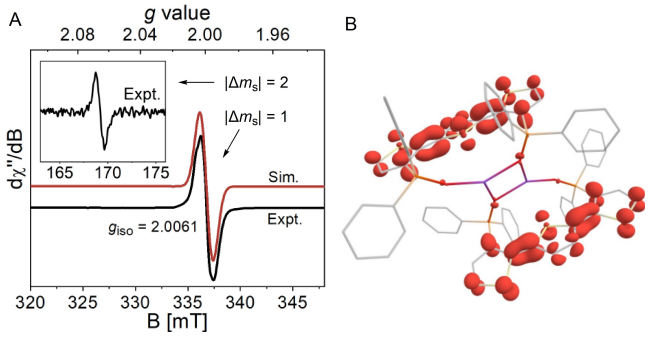


***Figure 1.*** A) X-band EPR spectrum of [Na(**2**)(THF)]$_2$ recorded in 2-Me-THF glass at 113 K. B) Spin density plot of [Na(**2**)]$_2$ from a gas-phase DFT calculation at the BP86 level of theory. See Supporting Information for full spin population analysis.

suggest that the electronic structure of [Na(**2**)(THF)]$_2$ is likely best described as approaching a quinoidal bonding scenario (**2**$^{\bullet-}$ in Scheme 2D). [Na(**2**)(THF)]$_2$ can therefore be viewed as a structurally characterized model for reductively-doped (n-type) oligothiophenes.[21]

Magnetic and spectroscopic measurements were carried out on [Na(**2**)(THF)]$_2$ to gain additional insight into its electronic structure. A magnetic moment of $2.31 \pm 0.03\ \mu_B$ was measured at room temperature in THF solution (Evans method) that is consistent with an $S=1$ ground state and implies that the dimeric structure observed in the solid-state for [Na(**2**)(THF)]$_2$ persists in solution. The X-band electron paramagnetic resonance (EPR) spectrum of [Na(**2**)(THF)]$_2$ was collected in 2-Me-THF glass at 113 K and exhibits an isotropic signal ($g_{iso}=2.0061$) in the $|\Delta m_s|=1$ region (Figure 1A). The formally forbidden half-field transition ($|\Delta m_s|=2$) is significantly less intense but was also observable at 113 K (Figure 1A, inset). Taken together, these data support the formulation of [Na(**2**)(THF)]$_2$ as an open-shell diradical[33] species with SOMOs delocalized across both terthiophene π-systems, a view that is also supported by the DFT-computed spin density plot of its geometry-optimized structure (Figure 1B). The observed structural, magnetic and spectroscopic features of [Na(**2**)(THF)]$_2$ thus establish the redox-responsive nature of phosphine oxide-functionalized TTH.

The identification of terthiophene-based reduction events in **2** prompted exploration of substituent effects for modulation of its electrochemical properties. Specifically, the installation of substituents at the TTH 5- and 5″-positions were pursued due to the influence of these activated sites on the terthiophene π-system electronics. Shown in Scheme 4A, di-lithiation of **2** followed by reaction with 2.0 equivalents of MeI afforded 5,5″-Me$_2$-3,3″-(P(O)Ph$_2$)$_2$-TTH (**3**) in 39 % yield. Bromination of **2** with NBS yielded the 5,5″-dibromo analog **4** in 92 % yield which was subsequently subjected to Pd-catalyzed Suzuki–Miyaura cross-coupling conditions to furnish the corresponding 5,5″-Ph$_2$-3,3″-(P(O)Ph$_2$)$_2$-TTH (**5**) in 45 % yield. Compounds **3** and **5** are yellow-orange solids that are luminescent in solution, generating emission maxima in the range 470–520 nm upon excitation at wavelengths corresponding to their main electronic absorptions ($\lambda_{max}=365$–$395$ nm; Figure S42). As in the case of **2**, two closely-matched cathodic redox couples were observed for both **3** and **5** that retain reversible character after 100 CV cycles at room temperature in DME (Figures S30, S32). While the $E_{1/2}$ values shift cathodically to −2.19 and −2.45 V vs Fc/Fc$^+$ for **3** relative to **2**, extension of the terthiophene π-system via the phenyl substituents in **5** resulted in an anodic shift of the potentials to −1.97 and −2.17 V. As summarized in Scheme 4A, the electrochemical properties of the compound series were hence tunable by straightforward structural derivatization.

Isolation of a doubly-reduced phosphine oxide-functionalized terthiophene was targeted to complete the 2 e$^-$ redox series. Although chemical reductions using Na[C$_{10}$H$_8$], KC$_8$ or Mg[C$_{14}$H$_{10}$] did not yield isolable dianionic species, controlled-potential electrolysis of **5** at −2.08 and −2.32 V enabled structural characterization of its singly- and doubly-

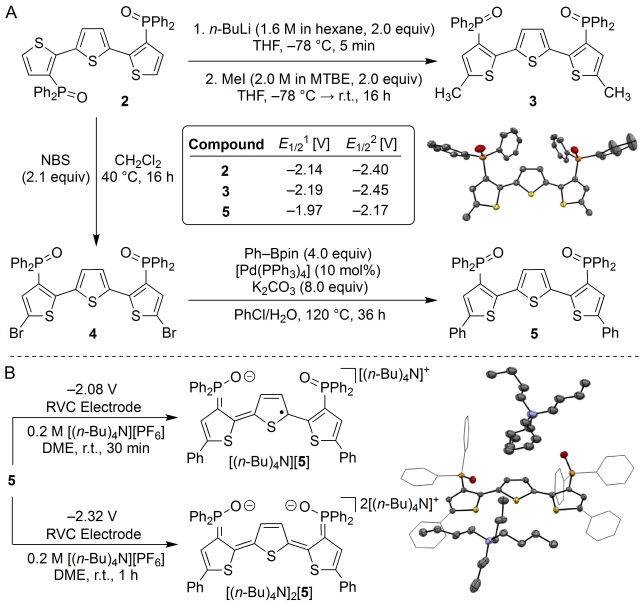


***Scheme 4.*** A) Synthesis and cathodic redox couples of **3** and **5** observed by CV recorded at 100 mV s$^{-1}$ (r.t., 1.0 mM compound, 0.10 M [(*n*-Bu)$_4$N][PF$_6$] in DME, glassy carbon working electrode) together with the solid-state structure of **3** with 50% probability ellipsoids (hydrogen atoms omitted). B) Controlled-potential electrolysis of **5** to generate [(*n*-Bu)$_4$N][**5**] and [(*n*-Bu)$_4$N]$_2$[**5**] (see Supporting Information for details) together with the solid-state structure of [(*n*-Bu)$_4$N]$_2$[**5**] with 50% probability ellipsoids (hydrogen atoms omitted, phenyl substituents represented without probability ellipsoids for clarity).

reduced analogs **5**$^{\bullet-}$ and **5**$^{2-}$, respectively, as [(*n*-Bu)$_4$N]$^+$ salts (Scheme 4B). The radical species [(*n*-Bu)$_4$N][**5**] exhibits a monomeric solid-state structure and consequently an isotropic EPR signal in 2-Me-THF glass without a half-field transition ($g_{iso}$ = 2.0039, Figure S47). The terthiophene bond lengths in the solid-state structure of [(*n*-Bu)$_4$N][**5**] were found to be comparable to those in [Na(**2**)(THF)]$_2$ as a consequence of one-electron reduction. By contrast, [(*n*-Bu)$_4$N]$_2$[**5**] was found to distort towards a fully quinoidal form and its solid-state structural metrics were best reproduced in a DFT-optimized geometry of **5**$^{2-}$ having a closed-shell ($S$ = 0) ground state (Table S3). Both [(*n*-Bu)$_4$N][**5**] and [(*n*-Bu)$_4$N]$_2$[**5**] were found to be stable in solution at room temperature in an Ar-filled glovebox as evidenced by minor attenuation of their characteristic CV features over the course of 2 days (Figures S39, S40). These results underscore the remarkable robustness of charged phosphine oxide-functionalized terthiophenes and provide insight into the structural features of a 2 e$^-$ redox series.

Galvanostatic charge–discharge cycling experiments were conducted to test the bulk redox stability of the phosphine oxide-functionalized terthiophenes. We employed an H-cell setup for this purpose, which is an established method for evaluating the suitability of redox systems for bulk energy storage as RFB electrolytes.[11,12,15,34,35] In contrast to 1 e$^-$ cycling, achieving robust 2 e$^-$ cycling in H-cells is challenging due to the co-existence of several highly reactive redox species that can participate in side-reactions during the long timescale of the cycling experiment.[13] This problem is further exacerbated at extreme negative potentials and also by any separation of the redox couples wherein large $E_{1/2}$ differences can result in significant voltaic efficiency losses.[36] Although compounds **3**–**5** all feature closely-matched cathodic redox couples, **5** was selected for H-cell experiments as it exhibits the smallest potential difference between its first and second reductions ($\Delta E_{1/2}$ = 0.20 V) as well as the most favorable solubility properties.[37]

In a symmetric H-cell with in situ generated **5**$^{2-}$ (1.0 mM, 0.20 M [(*n*-Bu)$_4$N][PF$_6$] in DME), a constant current of ±0.5 mA (2 C) was applied using reticulated vitreous carbon (RVC) working- and counter-electrodes. To access the cathodic redox couples of **5** (Figure 2A, inset), the voltaic cutoffs during H-cell cycling were set to −2.47 V and −1.37 V vs Fc/Fc$^+$ for charging and discharging, respectively. Shown in Figure 2A, starting from an initial state of charge (SOC) of 73.7%, over the course of 46 hours (50 cycles), >98% Coulombic efficiency was maintained and 91% of the initial capacity of **5** was preserved. These metrics translate to a remarkably low capacity fade of 0.15% per hour for **5**.[38] The profile of the cell voltage during cycling was found to be consistent with the CV data, further supporting stable 2 e$^-$ cycling at the expected potentials (Figure 2B). Given the strongly reducing nature of both redox couples cycled, **5** offers improved theoretical

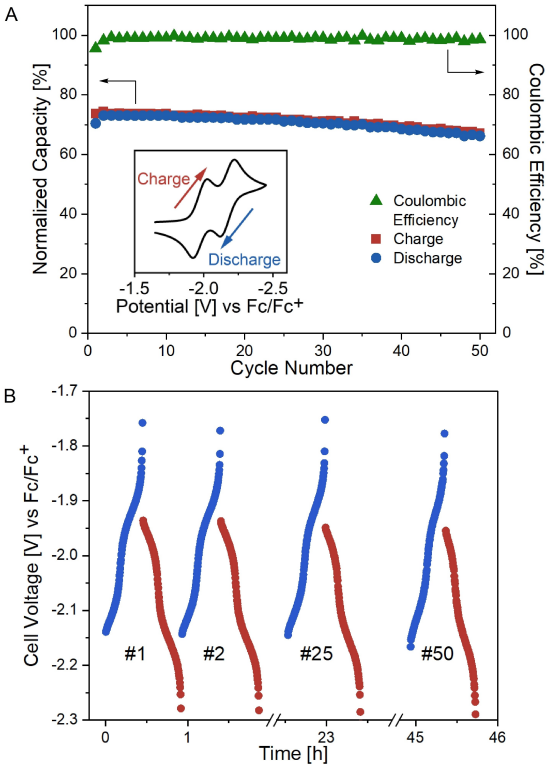


***Figure 2.*** A) Normalized cell capacity and Coulombic efficiency vs cycle number for the 2 e$^-$ charge/discharge cycling of **5**$^{2-}$/**5** in a symmetric H-cell. Inset: CV of **5**. B) Cell voltage profile of the **5**$^{2-}$/**5** charge/discharge process (see Supporting Information for details).

cell voltage over state-of-the-art organic redox systems together with ca. 5× lower capacity fade (Figure S41). This exceptional combination of stored electrochemical energy and stability thus serves as a key proof-of-concept and suggests that phosphine oxide-functionalized terthiophenes are a promising new class of main group electrolytes for RFB applications.

In summary, we have demonstrated that ubiquitous terthiophenes can be applied as robust $2e^-$ storage media by straightforward functionalization with phosphine oxides. An unusual phosphine oxide-functionalized terthiophene radical anion was isolated and its electronic structure was investigated by spectroscopic, computational, and single crystal X-ray diffraction methods. Modification of the terthiophene backbone led to the identification of a diphenyl-substituted derivative that exhibited exceptional stability at extreme negative potentials during bulk charge–discharge cycling and allowed structural characterization of a $2e^-$ redox series. We thus disclose a robust and modular $2e^-$ redox platform that expands the theoretical RFB cell potential window achievable with main group electrolytes and offers new parameter space for further exploration. Namely, the $R_2P(O)$ functionality is highly modular and can be leveraged to tune the molecular weights and solubilities of the redox systems in order to optimize their weight-to-charge ratios and energy densities.[39] Besides implementation as RFB electrolytes, phosphine oxide-functionalized terthiophenes may also be applied to advance main group electronics as conducting polymer precursors[40] and spin systems.[41]

## Acknowledgements

ETH Zürich and the Swiss National Science Foundation (SNSF 207390) are thanked for financial support. The authors gratefully acknowledge Prof. Dr. Hansjörg Grützmacher (ETH Zürich) for insightful discussions, and members of the Grützmacher laboratory for assistance during the start-up phase of the Bezdek group. The Molecular and Biomolecular Analysis Service (MoBiAS), X-ray (SMoCC) and NMR facilities of ETH Zürich are thanked for technical assistance. The Copéret laboratory (ETH Zürich) is acknowledged for providing access to EPR instrumentation. Open Access funding provided by Eidgenössische Technische Hochschule Zürich.

## Conflict of Interest

The authors declare no conflict of interest.

## Data Availability Statement

The data that support the findings of this study are available in the Supporting Information of this article.

**Keywords:** Electrochemistry · Electronic Structure · Functional Oligothiophenes · Main Group Radicals · Redox Chemistry

[1] *Main Group Strategies towards Functional Hybrid Materials* (Eds.: T. Baumgartner, F. Jaekle), Wiley, New York, **2018**.
[2] *Organic Redox Systems, Synthesis Properties and Applications* (Ed.: T. Nishinaga), Wiley, New York, **2016**.
[3] D. Raabe, *Chem. Rev.* **2023**, *123*, 2436.
[4] P. P. Power, *Chem. Rev.* **2003**, *103*, 789.
[5] Z. Feng, S. Tang, Y. Su, X. Wang, *Chem. Soc. Rev.* **2022**, *51*, 5930.
[6] J. Luo, B. Hu, M. Hu, Y. Zhao, T. L. Liu, *ACS Energy Lett.* **2019**, *4*, 2220.
[7] J. Winsberg, T. Hagemann, T. Janoschka, M. D. Hager, U. S. Schubert, *Angew. Chem. Int. Ed.* **2017**, *56*, 686.
[8] K. Gong, Q. Fang, S. Gu, S. F. Y. Li, Y. Yan, *Energy Environ. Sci.* **2015**, *8*, 3515.
[9] B. Hu, T. L. Liu, *J. Energy Chem.* **2018**, *27*, 1326.
[10] J. Huang, Z. Yang, M. Vijayakumar, W. Duan, A. Hollas, B. Pan, W. Wang, X. Wei, L. Zhang, *Adv. Sustainable Syst.* **2018**, *2*, 1700131.
[11] J. D. Griffin, A. R. Pancoast, M. S. Sigman, *J. Am. Chem. Soc.* **2021**, *143*, 992.
[12] C. S. Sevov, D. P. Hickey, M. E. Cook, S. G. Robinson, S. Barnett, S. D. Minteer, M. S. Sigman, M. S. Sanford, *J. Am. Chem. Soc.* **2017**, *139*, 2924.
[13] K. H. Hendriks, C. S. Sevov, M. E. Cook, M. S. Sanford, *ACS Energy Lett.* **2017**, *2*, 2430.
[14] C. R. Bridges, A. M. Borys, V. A. Béland, J. R. Gaffen, T. Baumgartner, *Chem. Sci.* **2020**, *11*, 10483.
[15] P. W. Antoni, C. Golz, M. M. Hansmann, *Angew. Chem. Int. Ed.* **2022**, *61*, e202203064.
[16] M. Stolar, C. Reus, T. Baumgartner, *Adv. Energy Mater.* **2016**, *6*, 1600944.
[17] I. F. Perepichka, D. F. Perepichka, H. Meng in *Handbook of Thiophene-Based Materials* (Eds.: I. F. Perepichka, D. F. Perepichka), Wiley, Chichester, **2009**, pp. 695–756.
[18] T. P. Kaloni, P. K. Giesbrecht, G. Schreckenbach, M. S. Freund, *Chem. Mater.* **2017**, *29*, 10248.
[19] A. Mishra, C.-Q. Ma, P. Bäuerle, *Chem. Rev.* **2009**, *109*, 1141.
[20] S. H. Oh, C.-W. Lee, D. H. Chun, J.-D. Jeon, J. Shim, K. H. Shin, J. H. Yang, *J. Mater. Chem. A* **2014**, *2*, 19994.
[21] M. Mastragostino, L. Soddu, *Electrochim. Acta* **1990**, *35*, 463.
[22] N. Zamoshchik, Y. Sheynin, M. Bendikov, *Isr. J. Chem.* **2014**, *54*, 723.
[23] J. Casado, L. L. Miller, K. R. Mann, T. M. Pappenfus, H. Higuchi, E. Ortí, B. Milián, R. Pou-Amérigo, V. Hernández, J. T. López Navarrete, *J. Am. Chem. Soc.* **2002**, *124*, 12380.
[24] A. Facchetti, M.-H. Yoon, C. L. Stern, G. R. Hutchison, M. A. Ratner, T. J. Marks, *J. Am. Chem. Soc.* **2004**, *126*, 13480.
[25] L.-L. Chen, W.-Y. Tan, X.-H. Zhu, *Sci. Bull.* **2020**, *65*, 2033.
[26] T. Baumgartner, *Acc. Chem. Res.* **2014**, *47*, 1613.
[27] H. Bock, U. Lechner-Knoblauch, P. Hänel, *Chem. Ber.* **1986**, *119*, 3749.
[28] A. M. Kuchison, M. O. Wolf, B. O. Patrick, *Chem. Commun.* **2009**, 7387.
[29] A. M. Kuchison, M. O. Wolf, B. O. Patrick, *Dalton Trans.* **2011**, *40*, 6912.
[30] T. P. Kaloni, G. Schreckenbach, M. S. Freund, *J. Phys. Chem. C* **2015**, *119*, 3979.
[31] G. Grover, J. D. Tovar, M. Kertesz, *J. Phys. Chem. C* **2022**, *126*, 5302.
[32] Deposition Numbers 2250509 (for $[Na(\mathbf{2})(THF)]_2$), 2250510 (for **2**), 2250511 (for **4**), 2250512 (for **3**), 2260027 (for $[(n\text{-}Bu)_4N][\mathbf{5}]$) and 2260028 (for $[(n\text{-}Bu)_4N]_2[\mathbf{5}]$) contain the supplementary crystallographic data for this paper. These data

are provided free of charge by the joint Cambridge Crystallographic Data Centre and Fachinformationszentrum Karlsruhe Access Structures service.
[33] N. Gallagher, H. Zhang, T. Junghoefer, E. Giangrisostomi, R. Ovsyannikov, M. Pink, S. Rajca, M. B. Casu, A. Rajca, *J. Am. Chem. Soc.* **2019**, *141*, 4764.
[34] G. D. De La Garza, A. P. Kaur, I. A. Shkrob, L. A. Robertson, S. A. Odom, A. J. McNeil, *J. Mater. Chem. A* **2022**, *10*, 18745.
[35] L. E. VanGelder, A. M. Kosswattaarachchi, P. L. Forrestel, T. R. Cook, E. M. Matson, *Chem. Sci.* **2018**, *9*, 1692.
[36] B. J. Neyhouse, A. M. Fenton, Jr., F. R. Brushett, *J. Electrochem. Soc.* **2021**, *168*, 050501.
[37] The solubilities of **2**, **3** and **5** in DME were measured to be approximately 2, 7 and 17 mM, respectively.
[38] For a discussion on capacity fade per hour as the preferred metric for cell stability, see: J. A. Kowalski, B. J. Neyhouse, F. R. Brushett, *Electrochem. Commun.* **2020**, *111*, 106625.
[39] R. M. Darling, K. G. Gallagher, J. A. Kowalski, S. Ha, F. R. Brushett, *Energy Environ. Sci.* **2014**, *7*, 3459.
[40] T. M. Swager, *Macromolecules* **2017**, *50*, 4867.
[41] B. C. Streifel, J. L. Zafra, G. L. Espejo, C. J. Gómez-García, J. Casado, J. D. Tovar, *Angew. Chem. Int. Ed.* **2015**, *54*, 5888.

Manuscript received: March 31, 2023
Accepted manuscript online: May 16, 2023
Version of record online: June 7, 2023